Light field imaging with a gradient index liquid crystal microlens array

Lei Yu[1,2], Tong Qing[1], Zhang Xinyu[1]

(1. School of Automation, Huazhong University of Science & Technology, Wuhan 430074, China;
2. School of Information Science & Technology, Shijiazhuang Tiedao University, Shijiazhuang 050043, China)

Abstract: Light field imaging is an imaging method which can acquire the three-dimensional information of the scene. By inserting a microlens array between the main lens and the imaging sensor, it records both the radiance and the direction of the incident rays. Light field imaging using a gradient index liquid crystal microlens array (LCMLA) was proposed. Based on nematic liquid crystal materials for their anisotropy and birefringence, the LCMLA with a pattern of a circular-hole array was fabricated using ultraviolet lithography and wet etching. When an alternate voltage signal was applied between the two electrodes of the LCMLA, each microlens can converge incident rays effectively. An experimental system was set up to verify its focusing performance and measure its focal length. Then the LCMLA was assembled with a main lens and an imaging sensor to construct a light field imaging camera. Raw images were taken using the camera based on LCMLA.

Key words: light field imaging; liquid crystal microlens array; gradient index

CLC Number: TN256 **Document code:** A **DOI:** 10.3788/IRLA201746.0220002

使用梯度折射率液晶微透镜阵列的光场成像

雷 宇[1,2],佟 庆[1],张新宇[1]

(1. 华中科技大学 自动化学院,湖北 武汉 430074;
2. 石家庄铁道大学 信息科学与技术学院,河北 石家庄 050043)

摘 要: 光场成像可以获取场景的三维信息。通过在主透镜和图像传感器之间插入一个微透镜阵列,不仅可以记录光线的辐射度,还记录了光线入射的方向。提出了使用梯度折射率液晶微透镜阵列进行光场成像的方法。该阵列基于向列相液晶材料,利用其各向异性和双折射的特点,通过紫外光刻技术和湿法刻蚀技术制作,具有圆孔阵列图案。在该阵列的上下电极之间加载一个交流电压信号后,每个微透镜可以有效会聚入射光,搭建了测试系统来测试该阵列的聚焦特性和焦距。将该阵列与一个主透镜和一片图像传感器耦合得到一个光场成像相机,并使用该相机采集了图像。

关键词: 光场成像; 液晶微透镜阵列; 梯度折射率

收稿日期: 2016-06-11; **修订日期:** 2016-07-22

基金项目: 国家自然科学基金(61176052, 61432007);中央高校基本科研业务费专项资金(2014CG008);高等学校博士学科点专项科研基金(20130142110007);中国工程物理研究院太赫兹科学技术基金(CAEPTHZ201402)

作者简介: 雷宇(1977-),男,讲师,博士,主要从事光场成像方面的研究工作。Email:leiyu4983@126.com

通讯作者: 张新宇(1965-),男,教授,博士生导师,主要从事微纳光学器件制作方面的研究工作。Email:x_yzhang@hust.edu.cn

0 Introduction

With the rapid development of three-dimensional (3D) imaging technologies, light field imaging has gained much popularity in recent years. Unlike the conventional imaging method that records two-dimensional (2D) light radiance over photographic films or imaging sensors, the light field imaging captures the 3D light fields of scenes involving the radiance power and the ray direction. By 2D projections of the light field, traditional images focused on different planes and observed from different points of view can be recovered from the snapshot of the scene. Light field imaging has its roots in the integral photography methods, which were first described by Lippmann in 1908 [1]. Adelson and Wang proposed a type of plenoptic camera and built the first prototype in 1992 [2]. Ng et al. continuously improved it and then built the first hand-held plenoptic camera[3] in 2005 by inserting a microlens array (MLA) between the main lens and the imaging sensor. In 2009, Lumsdaine and Georgiev proposed a type of focused plenoptic camera[4] by changing the location of the MLA so as to focus on the real or virtual image produced by the main lens. Perwass and Wietzke presented a multi-focus plenoptic camera using a hybrid integrated MLA consisting of three types of microlenses with different focal lengths and the same aperture[5].

In recent years, the liquid crystal (LC) microlens array (LCMLA) have sprang up as a good substitute for silica MLA. LCs are excellent electro-optical materials which have relatively large electrical and optical anisotropies. They are widely used in adaptive optics[6-7], grating[8], phase retarder[9], and so on. Nematic LCs is generally used in the area of LC lens whose molecules are rod-like. In nematics, the long molecule axes are preferably oriented in one direction. If nematic LCs are sealed in a lens-shape cell, the directions of the LC molecules will reorient along the electric field direction in an electric field excited. Moreover, if the applied electric field is nonuniform, the tilting angles of each molecule can vary with the density of the electric field so as to form a gradient index (GRIN) lens. The first LC lens was fabricated by Sato in 1979[10]. After that, Nose and Sato prepared a LC microlens with a hole-patterned electrode and an indium-tin-oxide (ITO) coated counter electrode to generate a non-uniform electric field[11]. To date, a number of researchers have designed LC lens or LCMLA with different structure, material or process in various fields[12-16].

In this paper, we proposed a light field imaging camera using a LCMLA. We fabricated a LCMLA using nematic LCs and carried out experiments to prove that each of the LC lenses of the LCMLA can act as a GRIN lens for converging rays. Moreover, the focal length of the LCMLA is measured. The LCMLA was applied in a light field camera to test its real imaging capability. Raw images of the scene were taken by the device which give proof to the efficient work of the LCMLA.

1 Light field imaging

1.1 Radiance denotation

To characterize the light field camera, we introduce a denotation for processing rays following the development of Lumsdaine and Georgiev [17]. First, a plane perpendicular to the optic axis is given, and the light field radiance is defined as $R(q, p)$, where q and p are vectors representing the position and the direction respectively. The light power converging at a single point is an integral of radiance from all directions at this point, as given by the definition of

$$I(q)=\int_p \mathrm{R}(q,p)\mathrm{d}p \tag{1}$$

As Fig.1 shows, the denotation can be further simplified as a 2D form of

$$I(\theta)=\int_\theta R_x(x,\theta)\mathrm{d}\theta \tag{2}$$

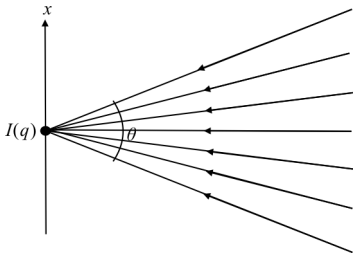

Fig.1 2D denotation of the radiance

1.2 Architecture and geometry

The architecture of a light field camera using a MLA is shown in Fig.2. The light field camera contains three components, the main lens, the MLA, and the imaging sensor. The main lens generates an image that lies somewhere to the left of it, which is then projected by the lenses of the MLA onto the imaging sensor. The main lens and the MLA constitute two imaging subsystems.

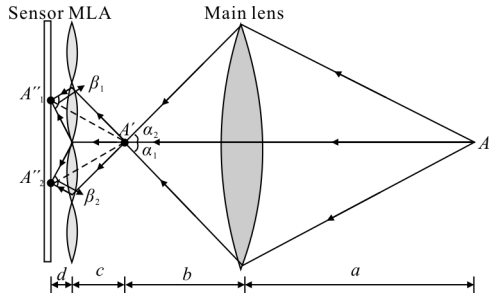

Fig.2 Architecture of a light field camera

As far as the object point A is concerned, it is imaged by the main lens to the image point A' at first. There is not an imaging sensor to collect the incident rays at the plane of A', so the rays from A' go ahead to the MLA and are focused by two adjacent microlenses to A''_1 and A''_2. Considering the main lens imaging system, it satisfies the thin lens equation:

$$\frac{1}{a}+\frac{1}{b}=\frac{1}{f_M} \tag{3}$$

where a, b, and f_M represent the object distance, the image distance, and the focal length of the main lens respectively. The radiance of the image point A' is

$$I(A')=\int_{\alpha_1+\alpha_2} R(x,\theta)\mathrm{d}\theta \tag{4}$$

As for the MLA imaging system, it also satisfies the thin lens equation:

$$\frac{1}{c}+\frac{1}{d}=\frac{1}{f_A} \tag{5}$$

where c, d, and f_A denote the object distance, the image distance, and the focal length of the microlenses. The radiances of the image point A''_1 and A''_2 on the sensor are

$$I(A''_1)=\int_{\beta_1} R(x,\theta)\mathrm{d}\theta\ ,\ I(A''_2)=\int_{\beta_2} R(x,\theta)\mathrm{d}\theta \tag{6}$$

It is obvious that the rays of A''_1 are from the rays of A' in the angle of α_1, and A''_2 from α_2, which means that the MLA separate the incident rays according to their directions. If the MLA is closer to A', more image points on the imaging sensor might be captured, and vice versa.

Therefore, the light field imaging method can acquire both the radiance and the direction of the rays. After one snapshot, the images of the original scene from different viewpoints or focused at different depths can be recovered through computation. The 3D model may also be setup according to the raw image. The algorithms of image processing is described in [17-20].

2 LCMLA

2.1 LC

A LC material is a kind of uniaxial birefringent crystals. Depending on the amount of order in the materials, there are nematic phases, smectic phases, cholesteric phases, and columnar phases. The nematic LCs are generally used in the fabrication of LC lenses. The LC molecules for nematic is rod-like and the optic axis is along the long axis. The optic axis will reorient along the direction of the outer electric field or magnetic field. LC materials have two principle refractive indexes, the ordinary index n_o and the extraordinary index n_e. When the electric vector of the light waves vibrates perpendicular to the optic axis, the refractive index is n_o. When along the optic axis, that is n_e. Generally $n_e>n_o$. When the light propagation direction

is tilted according to the optical axis, the refractive for the ordinary waves is equal to n_o, whereas the refractive index n_{eff} for extraordinary waves is as the following equation

$$n_{\text{eff}}(\theta)=\frac{n_o n_e}{\sqrt{n_e^2\cos^2\theta+n_o^2\sin^2\theta}} \tag{7}$$

where θ represents the angle between the optical axis and the light propagation direction.

2.2 LC circular hole microlens

The 3D structure of a LC circular hole microlens is shown in Fig.3 (a). It contains two electrodes on the substrates. The top electrode is an electrode with a circular hole in the center, and the bottom one is a planar electrode. The two substrates are conglutinated together tightly with adhesive along the edges. The nematic LCs are instilled between the two substrates mentioned above. When a certain alternating current(AC) voltage signal is applied over the electrodes, a symmetrical inhomogeneous electric field will be generated in the LC layer where the electric field intensity decreased gradually from the edges of the hole to the center. The LC molecules tend to reorient along the direction of the electric field, as shown in Fig.3(b). Therefore, the refractive index for extraordinary waves increases from n_e in the central region to n_o along the edges gradually. Finally, a GRIN microlens is shaped which can converge incident rays effectively.

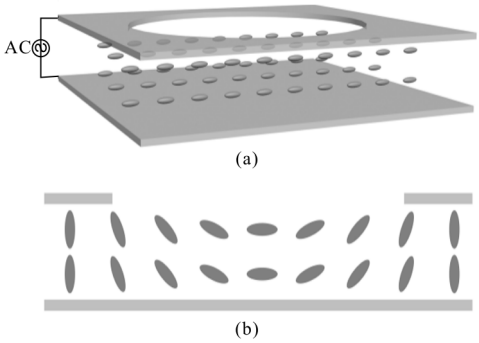

(a)

(b)

Fig.3 LC lens circular hole electrode

2.3 Structure of LCMLA

The 3D structure of the LCMLA is shown in Fig.4(a). It contains two electrodes with LC materials sandwiched in them. The top electrode is a 500 μm thick glass substrate with a thin aluminum layer sputtered on it. The aluminum layer is etched with an array of circular holes through ultraviolet lithography and wet etching. The diameter of the holes is 128 μm and the center-to-center distance is 160 μm. Then a ~80 nm thick polyimide (PI) layer is coated as the alignment layer through spinning coating. After that, the electrode is rubbed to form V-grooves on the PI layer so that the LC molecules will aligned homogeneously. The bottom electrode is another 500 μm thick glass substrate with a thin ITO layer on it. A PI layer is also coated on it and rubbed. Then the two electrodes are stick face to face with glue along the edges. The glue is mixed with 50 μm diameter glass microspheres to form a cavity between the electrodes where LC materials is instilled. The LC materials we used is E44 from Merck Group. The refractive indexes of the LCs are $n_e=1.778$ and $n_o=1.523$. Figure 4(b) shows a finished LCMLA with conductive tape to connect the electrodes with the wires from the electric source.

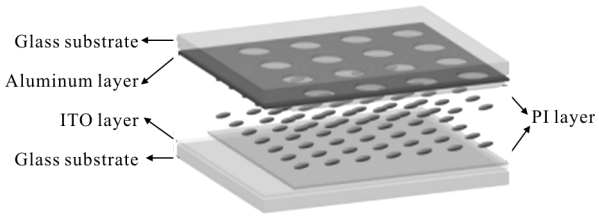

(a)

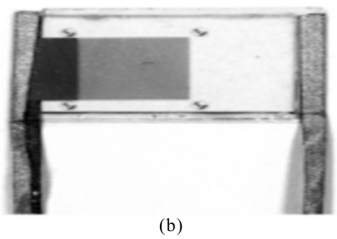

(b)

Fig.4 3D structure of actual LCMLA

2.4 Focusing performance

An experimental setup is configured to test the focusing performance of the LCMLA, as shown in Fig.5. A laser with a wavelength of 550 nm is used as the light source. The incident rays pass through

two polarizers after emitted to be effectively weakened. Then the weakened rays pass through the LCMLA whose power is supplied by an alternating current (AC) with a frequency of 1 kHz and adjustable voltages. The LCMLA will converge incident rays when its electrodes is applied with a voltage signal. After that, the optical field behind the LCMLA will be exaggerated by a 20× microscope and captured by a beam profiling camera (DataRay WinCamD). At last, the data is input into a computer to be analyzed.

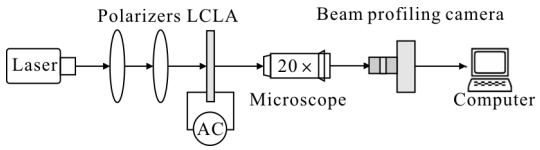

Fig.5 Setup to test the focusing performance of the LCMLA

When a voltage signal is applied between the electrodes of the LCMLA, the LC molecules begin to swing according to the electric field excited and a GRIN converging microlens array is formed instantly. The distance of the LCMLA and the microscope can be adjusted finely so that the optical fields at different distances from the LCMLA can be acquired and then the focal length of the LCMLA can be measured. Figure 6 shows the focusing fields of a certain microlens acquired when the applied voltage signal is ~5.0 Vrms (root-mean-square voltage) at different distances from the LCMLA. As is shown that the energy of the incident collimated rays are converged by the microlens effectively and the focusing spot reaches the smallest at the distance of 1.4 mm which means that the focal length is 1.9 mm, the sum of the distance and the thickness of the glass substrate.

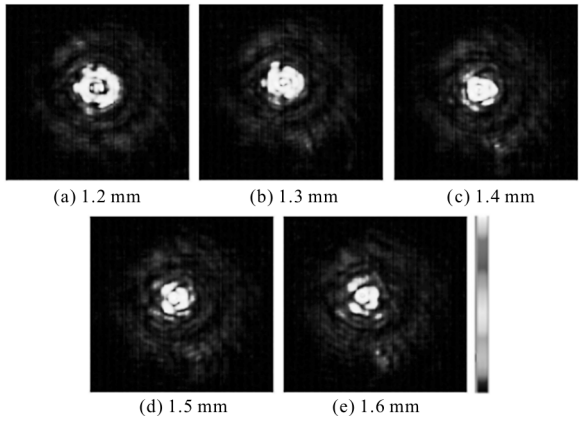

Fig.6 Optical fields of a microlens at different distances from the LCMLA when the applied voltage signals is ~5.0 Vrms

3 Experiments and results

We built a light field imaging camera using our LCMLA fabricated. The camera consists of three parts, the main lens, the LCMLA, and the imaging sensor. The resolution of the imaging sensor is 4 384× 3 288 with the pixel pitch of 1.4 μm. The arguments of the LCMLA is mentioned above and it is also driven by an AC of 1 kHz. The focal length of the main lens is 35 mm. Incident rays from the objects will be imaged by the main lens at first. Then the real image or virtual image will be projected by the LCMLA onto the imaging sensor. The distance from the main lens and the LCMLA can be adjusted to get the sharpest raw image. The LCMLA is fixed tightly on the protecting glass of the imaging sensor.

A toy car as the sample is placed before the imaging camera at a distance of ~40 cm. The LCMLA is applied with a voltage signal of ~5.0 Vrms and the light field camera begins to work efficiently. We adjusted the distance between the main lens and the LCMLA carefully. When the LCMLA is ~3.5 cm behind the main lens, a fairly sharp light filed raw image is acquired, as shown in Fig.7. It is obvious that each LC microlens focus the incident rays passing through it and project them onto the sensor. The

Fig.7 Raw image of a toy car when the applied voltage signal is ~5.0 Vrms

elemental image formed by each microlens occupies 114×114 pixels, and the sum of the elemental images is 38×30. To exhibit the details of the raw image more clearly, Figure 8 shows several elemental images cropped from the whole raw image. It is evident that the LCMLA have fairly good imaging capabilities and elemental images projected by adjacent microlenses are overlapped. However, the incident rays of overlapped region are from different directions. In this snapshot, the elemental images are erect because each microlens images the virtual image formed by the main lens. On the other hand, if the LCMLA image the real image of the main lens, each elemental image is inverted.

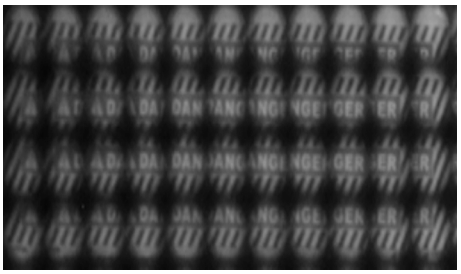

Fig.8 Several elemental images cropped from the whole raw image

4 Conclusion

In this paper, we fabricated a GRIN MLA based on nematic LC materials by ultraviolet lithography and wet etching. The LCMLA we fabricated can focus incident rays effectively. It is assembled into a light field imaging camera with a main lens and an imaging sensor, which can be used to acquire light field image. However, the images projected by LC microlenses are not as clear as that of silica microlenses. The focusing capability of LC lenses need to be improved and more experiments should be carried out to expand its applications in the area of light field imaging.

References:

[1] Lippmann G. Epreuves reversibles donnant la sensation du relief[J]. ***J Phys Theor Appl***, 1908, 7(1): 821-825.

[2] Adelson E H, Wang J Y. Single lens stereo with a plenoptic camera[J]. ***IEEE Trans Pattern Anal Mach Intell***, 1992, 14 (2): 99-106.

[3] Ng R, Levoy M, Brédif M, et al. Light field photography with a hand-held plenoptic camera [J]. ***Stanford Tech Rep***, 2005, 2: 1-11.

[4] Lumsdaine A, Georgiev T. The focused plenoptic camera[C] //Proceddings of IEEE International Conference on Computational Photography, 2009: 1-8.

[5] Perwass C, Wietzke L. Single lens 3D-camera with extended depth-of-field[C]//Proc SPIE, 2012, 8291: 829108.

[6] Liu Lili, Huang Tao, Cai Min, et al. Retinal imaging system with large field of view based on liquid crystal adaptive optics [J]. ***Optics and Precision Engineering***, 2013, 21(2): 301-307.(in Chinese)

[7] Wei Peifeng, Liu Xinyue, Lin Xudong, et al. Temporal simulation of atmospheric turbulence during adaptive optics system testing[J]. ***Chinese Optics***, 2013, 6(6): 371-377. (in Chinese)

[8] Huang Chong, Ouyang Yandong. Liquid crystal grating with variable and electrically controlled constants [J]. ***Chinese Optics***, 2012, 5(3): 296-301. (in Chinese)

[9] Zhang Ying, Zhao Haibo. Liquid crystal variable retarder attached with compensator [J]. ***Optics and Precision Engineering***, 2009, 17(8): 1798-1803. (in Chinese)

[10] Sato S. Liquid-crystal lens-cells with variable focal length [J]. ***Jpn J Appl Phys***, 1979, 18(9): 1679-1684.

[11] Nose T, Sato S. A liquid crystal microlens obtained with a non-uniform electric field[J]. ***Liq Cryst***, 1989, 5(5): 1425-1433.

[12] Kao Y Y, Chao P C P, Hsueh C W. A new low-voltage-driven GRIN liquid crystal lens with multiple ring electrodes in unequal widths [J]. ***Opt Express***, 2010, 18 (18): 18506-18518.

[13] Fan Y H, Ren H, Liang X, et al. Liquid crystal microlens arrays with switchable positive and negative focal lengths[J]. ***J Disp Technol***, 2005, 1(1): 151-156.

[14] Kang S, Qing T, Sang H, et al. Ommatidia structure based on double layers of liquid crystal microlens array [J]. ***Appl Opt***, 2013, 52(33): 7912-7918.

[15] Lei Yu, Tong Qing, Zhang Xinyu, et al. Plenoptic camera based on a liquid crystal microlens array [C]//Proc SPIE, 2015, 9579: 95790T.

[16] Tong Qing, Rong Xing, Zhang Xinyu, et al. Large-area

arrayed liquid crys tal device for measuring and regulating polarization state of incident light [J]. ***Infrared and Laser Engineering***, 2014, 43(2): 474-478. (in Chinese)

[17] Georgiev T, Lumsdaine A. Focused plenoptic camera and rendering[J]. ***J of Electron Imaging***, 2010, 19(2): 021106.

[18] Lumsdaine A, Lin L, Willcock J, et al. Fourier analysis of the focused plenoptic camera [C]//Proc SPIE, 2013, 8667: 86671M.

[19] Hahne C, Aggoun A, Haxha S, et al. Light field geometry of a standard plenoptic camera [J]. ***Opt Express***, 2014, 22 (22): 26659-26673.

[20] Zhang W, Guo X, You S, et al. Computer simulation for hybrid plenoptic camera super-resolution refocusing with focused and unfocused mode [J]. ***Infrared and Laser Engineering***, 2015, 44(11): 3384-3392. (in Chinese)